Single-Molecule Assay of Biological Reaction in Femtoliter Chamber Array

Ryota Iino, Liza Lam, Kazuhito V. Tabata, Yannick Rondelez[1], and Hiroyuki Noji*

The Institute of Scientific and Industrial Research, Osaka University, 8-1 Mihogaoka, Ibaraki, Osaka 567-0047, Japan
[1]*Institute of Industrial Science, University of Tokyo, 4-6-1 Komaba, Meguro, Tokyo 153-8505, Japan*

Received January 15, 2009; accepted March 2, 2009; published online August 20, 2009

We previously developed micron-sized, femtoliter (fL) reaction chamber array made of polydimethylsiloxane and polyacrylamide. Downsizing of the reaction volume to fL level made it possible to carry out single-molecule assay (SMA) of biological reactions in a straightforward manner. In this review, preparation of the fL chamber array and its application to SMA of enzyme, DNA, and rotary motor protein under an optical microscope are described. © 2009 The Japan Society of Applied Physics

DOI: 10.1143/JJAP.48.08JA04

1. Introduction

Recent advances in optical microscopy allowed us to carry out single-molecule assay (SMA) of biological reactions in aqueous environment at physiological temperature.[1–4] SMA of biological molecular machine like enzymes and motor proteins working under physiological condition is a powerful technique to understand their operation mechanism. SMA has been getting popular in last decade and excellent textbooks describing the details of methods have been published.[5,6] However, along with technical development, methods and instruments for SMA become more complex and expensive. There are still obstacles that make many people hesitate to try SMA. Development of simple, easy and cheap SMA will be appreciated by many non-expert researchers.

Another advance in the field of SMA is its combination with micro electro mechanical systems (MEMS) or micro total analysis systems (μTAS) technology.[7] Because the purpose of many applications of MEMS and μTAS to biology is the rapid diagnosis of diseases such as infection, highly sensitive measurement down to the single-molecule level is often preferred. Furthermore, combination of SMA with MEMS and μTAS can make it possible to achieve high throughput SMA while saving precious samples and expensive reagents.

Furthermore, downsizing of reaction volume using MEMS and μTAS technology has an additional important advantage. In short, smaller volume is better for highly sensitive detection of biological reaction. As an example, let's consider an enzyme with a turnover rate of $10\,s^{-1}$, corresponding to the generation of 600 product molecules per enzyme and per minute. If a single-molecule of this enzyme (together with its substrate) is enclosed in a volume of 1 μL (1 mm^3), the typical scale used in conventional biochemical assay, product concentration will increase at a rate of only 1 fM/min (10^{-15} M/min). This value is far below the detection limit of conventional assay. However, if reaction volume is decreased to 1 fL (1 μm^3), the rate significantly increases to 1 μM/min (10^{-6} M/min). This concentration is high enough for conventional method of product detection like fluorescence. This simple idea motivated us to develop micron-sized, femtoliter (fL) chamber array.[8]

By observing fL chambers under conventional optical microscope, SMA of biological reactions can be easily achieved. In this review, SMA of β-galactosidase activity is described as an example.[8] Furthermore, fL chamber array can be combined with other single-molecule methods. As examples, first, fragmentation by restriction enzyme, size measurement, and amplification of DNA are introduced.[9–11] Second, quantitative measurement of mechano-chemical coupling efficiency of a rotary motor protein F_1-ATPase is described.[12,13]

2. Preparation of fL Chamber Array

To prepare fL chamber array, a silicon plate with many microcavities (~10^5) on its surface was prepared first by conventional microfabrication method [Fig. 1(a)].[8] Silicon-on-insulator wafer was covered with an aluminum mask, which was patterned by photolithography. After etching and removing the aluminum layer, the silicon surface showed identical cylinders with diameters down to 1 μm, giving 1 fL in volume. On this mold, a liquid silicon elastomer, polydimethylsiloxane (PDMS) was poured and then polymerized. PDMS is transparent and nontoxic, and is convenient for observation of biological sample under an optical microscope.[14]

In this manner, a PDMS sheet with microcavity array was prepared [Fig. 1(b)]. To form fL reaction chambers, a droplet of the sample solution was placed on a coverglass and pressed with the PDMS sheet [Fig. 1(c)]. The PDMS sheet tightly binds to the coverglass surface through Van der Waals forces and hermetic reaction chambers can be easily formed. Figures 1(d)–1(f) shows images of 100 nm latex beads, 5 kbp DNA molecules, and living bacteria enclosed in fL chambers, respectively. The Brownian motion of the beads, or active swimming of the bacterias can be observed for more than 1 hour, which implies that evaporation does not occur at this time scale.

3. Application of fL Chamber Array to SMA

3.1 Measurement of β-galactosidase activity

With this fL chamber array, SMA of enzymatic activity of β-galactosidase (β-gal) was carried out as a model case.[8] We used fluorescein-di-β-D-garactopyranoside (FDG) as a fluorogenic substrate [Fig. 2(a)].[15] FDG is a non-fluorescent substrate that is converted into a fluorescent product, fluorescein, after cleavage by β-gal. So, the reaction can be monitored by increase in fluorescence intensity under an optical microscope. The FDG solution was mixed with a very low concentration of β-gal in order to decrease the probability that each chamber contains two or more β-gal molecules. Just after mixing, the reaction solution was

*E-mail address: hnoji@sanken.osaka-u.ac.jp

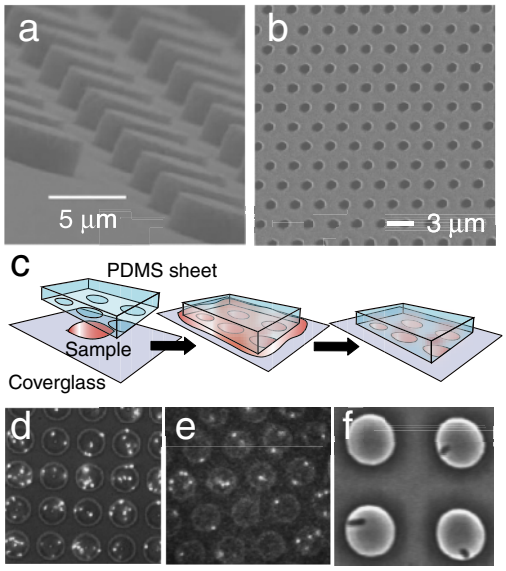

Fig. 1. (Color online) Preparation of fL chamber array. SEM images of the silicon mold with micron-sized cylinders (a) and the PDMS sheet with micron-sized cavities (b). (c) fL chambers can be easily formed by sandwiching the sample solution between the PDMS sheet with cavities and the coverglass. Images of 100 nm bead (d), 5 kbp DNA (e), and living bacteria (f) enclosed in fL chambers.

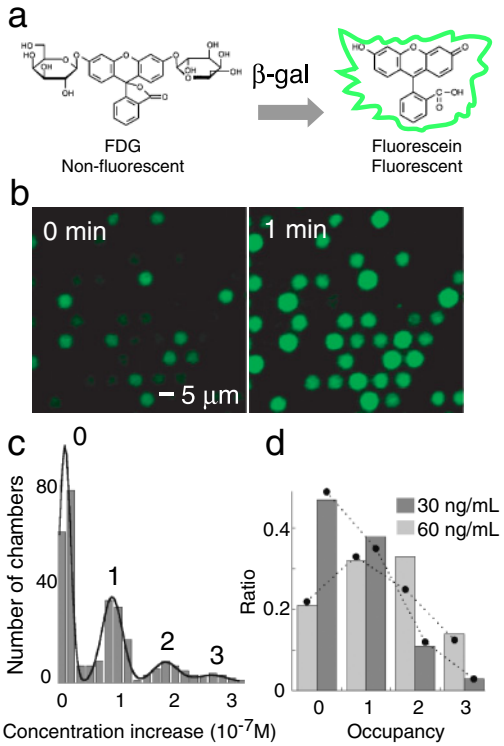

Fig. 2. (Color online) SMA of β-galactosidase (β-gal). (a) FDG used in this experiment. (b) Fluorescence images of fL chambers after enclosure of β-gal and FDG. (c) Distribution of increase in product (fluorescein) concentration for 1 minute. Each peak corresponds to chamber containing 0, 1, 2, and 3 β-gal molecules. (d) Ratio of chambers as a function of the number of β-gal molecules enclosed. Bars: experimental results. Circles: calculated values assuming the Poisson distribution.

enclosed in fL chamber array. Figure 2(b) shows the fluorescence images obtained just after enclosure (0 min, left) and 1 minute later (right), respectively. Increase in fluorescence intensity was clearly observed after only 1 min, indicating that these chambers contained one or more β-gal molecules. On the other hand, some chambers remained dark, indicating that they did not contain any β-gal molecules.

Distribution of product (fluorescein) concentration increment for 1 min in each chamber showed quantized peaks [Fig. 2(c)]. These peaks corresponded to the chambers that contain 0, 1, 2, and 3 β-gal molecules, respectively. The intervals between the peaks were almost equal and gave the catalytic rate of a single β-gal at $20\,s^{-1}$. This value was consistent with that estimated from ensemble-molecule measurement. In Fig. 2(d), the bars show the ratios of chamber containing 0, 1, 2, and 3 β-gal molecules at different concentrations. The measured ratio showed good agreement with that calculated assuming the Poisson distribution of β-gal in each chamber (black circles). Therefore, β-gal molecules seemed not to be denatured by nonspecific binding to the surface of PDMS or coverglass.

To confirm that most of β-gal in the chambers were really active, we carried out experiment in which chambers were reversibly opened and closed [Fig. 3(a)]. The PDMS sheet with fL cavity array was suspended above the coverglass using spacers. Then, PDMS sheet was partly pushed with a glass needle to close a few chambers. When the PDMS sheet contacted the glass surface, β-gal molecules were trapped, and the fluorescence intensity in some chambers started to increase. The glass needle was then pulled back up and chambers were opened to let the β-gal diffuse out. Images in Fig. 3(b) are successive images of the same area taken after each opening/closing cycle. Each time, the β-gal molecules were enclosed in different chambers, and the number of chambers containing β-gal was roughly constant. Therefore,

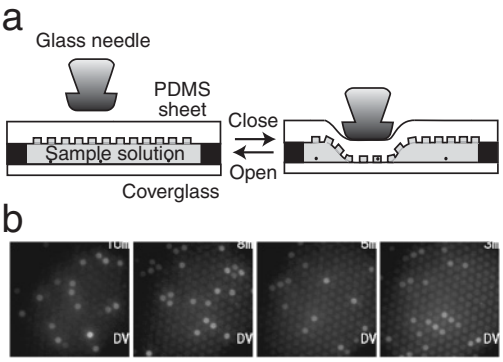

Fig. 3. Reversible enclosure of single β-gal molecules in fL chamber. fL chambers were formed reversibly by pressing a glass needle against the PDMS sheet. (a) Schematic drawing of experimental system. (b) Successive fluorescence images during repeated enclosures.

β-gal molecules were free in the chambers and were not denatured by enclosure. SMA described here also can be applied to other enzymes such as horseradish peroxidase, if appropriate fluorogenic substrate is available.

3.2 Restriction enzyme digestion, size measurement and, amplification of DNA

Restriction enzyme cleaves a specific recognition sequence of DNA by making an incision at the phosphate backbone of the double helix structure. These enzymes allow us to reproducibly cut DNA molecules into well-defined frag-

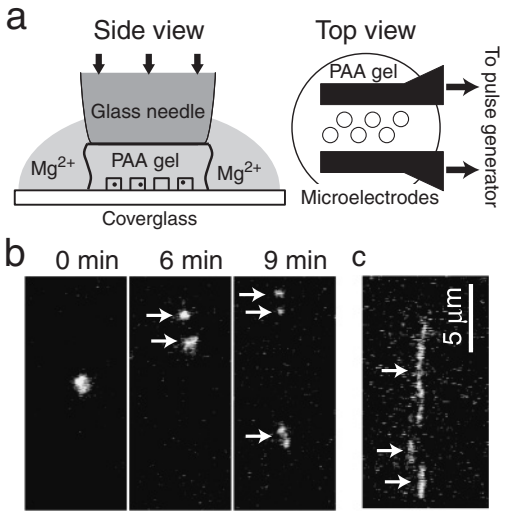

Fig. 4. DNA digestion by restriction enzyme and subsequent DNA electrostretching in fL chamber. (a) Schematic drawing of experimental setup. Reaction was triggered by externally added Mg^{2+} ion. (b) Digestion of λDNA by *PmeI*. The first and second cuts occurred at 6 and 9 minutes, respectively. (c) Subsequent electrostretching of the three DNA fragments (indicated by arrows) in the same fL chamber. An alternating electric field (1.2×10^3 V/cm at 1.5 kHz) was applied using a pair of microelectrodes.

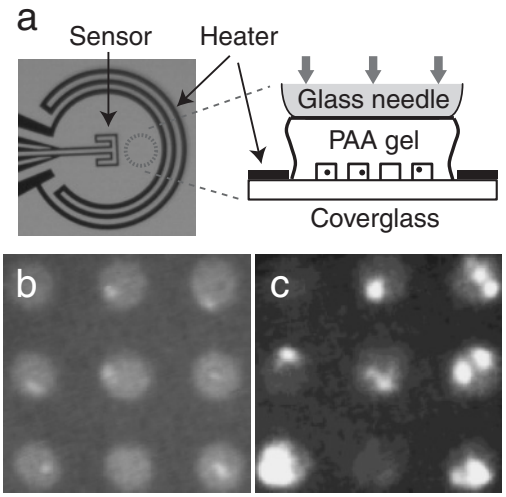

Fig. 5. LAMP of DNA in fL chamber. (a) Shematic drawing of experimental setup. The fL chambers containing DNA and primers for LAMP were incubated at 65 °C using a micro-heater. (b) Fluorescence image (averaged over 30 video frames) of DNA before amplification. (c) Fluorescence image (averaged over 200 video frames) after amplification for 50 min.

ments and are a powerful tool for gene manipulation and gene diagnosis. Recently, we developed a polyacrylamide (PAA) gel-based fL chamber system to carry out SMA of restriction enzyme.[9,11] This system consisted of enclosure and activation process [Fig. 4(a)]. Firstly, PAA gels were polymerized on the silicon mold with cylinders approximately 1.5 μm in height and 17 μm in diameter. As previously described, a sample solution containing fluorescently-stained λDNA molecules and restriction enzymes was put on a coverglass and enclosed in the chambers by pressing the PAA gel against the coverglass with a glass needle.

Restriction enzyme digestion was triggered externally by applying magnesium chloride ($MgCl_2$) solution on the exterior of the PAA gel upon complete enclosure. Mg^{2+} ions were allowed to diffuse through the porous PAA gel matrix and enter the fL chamber. The entire process was monitored in real-time and the individual cleaving events were captured as shown in Fig. 4(b). The time required to initiate digestion after addition of $MgCl_2$ on the PAA gel was approximately 6 min. Several simple modifications such as reducing the dimensions of the PAA gel and introducing an external DC current across the PAA gel can increase the initiation rate of the reaction several times.

To analyze the digested fragments in fL chambers, we employed DNA electrostretching [Figs. 4(a) and 4(c)].[16] Generally, DNA electrostretching is carried out under extremely low ionic strength conditions to prevent excessive heat dissipation and convection flow under the high electric field (10^3–10^4 V/cm). To enable the DNA electrostretching in the buffer containing ions at mM levels, we added linear PAA (LPA) to the solution.[17] Although the actual mechanism is still not clear, it has been proposed that the entanglement of LPA with DNA supports efficient electrostretching. An alternating electric field (1.2×10^3 V/cm at 1.5 kHz) was applied across the fL chambers using a pair of microelectrodes printed onto the underlying coverglass [Fig. 4(a), right]. These microelectrodes were connected to a pulse generator which supplies alternating signals with adjustable ranges of signal strengths and frequencies, hence enabling the determination of optimum stretching condition. Because the PAA gel matrix is porous to electric field penetration, DNA molecules enclosed in fL chambers could be easily manipulated.

In an attempt to demonstrate an integrated SMA system, DNA digestion by restriction enzyme was combined with subsequent DNA electrostretching within the same fL chamber [Figs. 4(b) and 4(c)]. Three different restriction enzymes (NheI, PmeI and BamHI) were used for digestion of λDNA molecule. Subsequent electrostretching of the cleaved fragments enabled the direct measurement of the lengths, which corresponded well with their respective theoretical sizes (up to 80% accuracy).

We have also carried out single-molecule loop-mediated isothermal amplification (LAMP) of DNA in PAA gel-based fL chambers (Fig. 5).[10] In this experiment, fluorescently-stained single DNA template in sample solution containing LAMP primers and buffers was heated with a microfabricated heater [Fig. 5(a)] and continuously monitored. After 50 min of incubation at 65 °C by localized heating using micro-heater [Fig. 5(a)],[18] high molecular weight amplified products were observed [Figs. 5(b) and 5(c)]. This result emphasize several advantages of fL chamber array such as the capability for direct visualization, lower sample consumption, rapid processing time, and simple implementation of electronics.

3.3 Quantitative measurement of mechano-chemical coupling efficiency of single F_1-ATPase

F_1-ATPase (F_1) is a rotary molecular motor made of protein.[19–21] Bacterial F_1 has a $\alpha_3\beta_3\gamma\delta\varepsilon$ subunit structure. Among these subunits, the $\alpha_3\beta_3\gamma$ subcomplex is the minimum functional unit as a rotary motor driven by ATP hydrolysis. Figure 6(a) shows the crystal structure of the

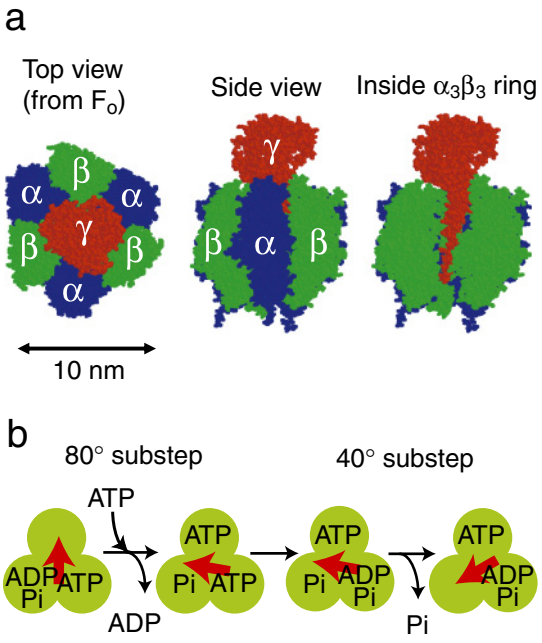

Fig. 6. (Color online) A rotary motor protein, F_1-ATPase. (a) Crystal structure of the $\alpha_3\beta_3\gamma$ subcomplex of F_1. The γ subunit is inserted into a ring formed by the $\alpha_3\beta_3$ subunits, and rotates within this ring upon ATP hydrolysis at β subunits. (b) A model of mechano-chemical coupling scheme of F_1. Three circles and an arrow represent the three β subunits and the γ subunit, respectively.

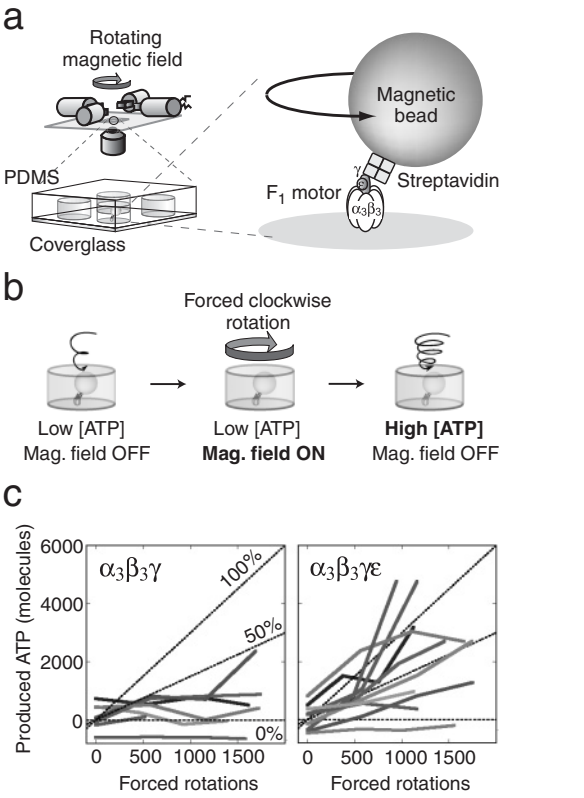

Fig. 7. SMA of mechano-chemical coupling efficiency of ATP synthesis by forced rotation of F_1. (a) Schematic drawing of experimental setup. (b) Experimental procedure of ATP synthesis. Single F_1 is enclosed in a fL chamber (left) and the rotation of the magnetic bead attached to γ is forced using magnetic tweezers (center). Newly synthesized ATP accumulates in the chamber. The number of synthesized ATP molecules is estimated from the increase in ATP-driven (free) rotational speed (right). (c) Number of ATP molecules synthesized by $\alpha_3\beta_3\gamma$ (left) and $\alpha_3\beta_3\gamma\varepsilon$ (right) subcomplexes of F_1 after forced rotation. Each trace belongs to individual F_1. Dotted lines indicate slopes of the coupling ratio of 0% (0 ATP/turn), 50% (1.5 ATP/turn), and 100% (3 ATP/turn), respectively.

$\alpha_3\beta_3\gamma$ subcomplex.[22] In this subcomplex, the $\alpha_3\beta_3$ ring creates a stator that allows the γ subunit to act as a rotor. Each β subunit carries a catalytic site and three β subunits sequentially and cooperatively hydrolyzes ATP.[23,24] The rotary motion of F_1 driven by ATP hydrolysis was visualized directly for the first time in 1997.[19] In this experiment, the stator was fixed on the glass surface to suppress the Brownian motion of F_1 in water, and a fluorescently-labeled actin filament, a micron-sized probe made of protein was attached to the rotor to amplify the small turning radius ($\sim$1 nm) of the γ subunit. Then, the rotation of the probe could be directly observed under a fluorescence microscope. In recent experiments, latex beads are often used as a rotational probe instead of the actin filament.[25]

By analyzing the rotational behavior of F_1 driven by ATP hydrolysis, many properties of this motor protein, such as rotary torque, maximum speed and detail of mechano-chemical coupling scheme have been revealed. F_1 rotates 120° by single ATP hydrolysis,[26] and each 120° step is further divided into 80 and 40° substeps [Fig. 6(b)].[27] The 80° substep is triggered upon ATP binding, whereas the 40° substep occurs after covalent bond cleavage.[27,28] The releases of reaction products, ADP and inorganic phosphate (P_i), are thought to occur before or during 80 and 40° substeps, respectively.[29,30] As described here, when F_1 hydrolyzes ATP, the rotation is tightly coupled with chemical reaction and 3 ATP molecules are hydrolyzed per turn.

However, the physiological role of F_1 is not ATP hydrolysis, but ATP synthesis.[31] For ATP synthesis *in vivo*, F_1 forms a complex with a partner, F_o, another rotary motor. F_o is embedded in cell membrane and its rotation is driven by the electrochemical potential gradient of proton across the membrane. With regard to the ATP synthesis reaction, it is widely accepted that when F_o forces the reverse rotation of F_1, chemical reaction is also reversed to generate ATP from ADP and P_i. This hypothesis was first experimentally supported by Itoh *et al.* who demonstrated that the reverse rotation of the $\alpha_3\beta_3\gamma$ subcomplex of F_1 led to ATP synthesis.[32] However, without knowing the number of active F_1 molecules in the reaction volume, it was difficult to determine the number of ATP molecules synthesized per turn and per F_1 molecule.

We addressed this issue by combining the fL chamber system and single-molecule manipulation of F_1 [Fig. 7(a)].[12] The task we had to achieve was to combine the mechanical rotation of F_1 in direction to the ATP synthesis, with the detection of the small amount of ATP synthesized by a single F_1 molecule. Mechanical rotation of F_1 can be easily carried out by using a magnetic bead as a probe of rotation and applying an external rotating magnetic field generated by two pairs of electromagnets (magnetic tweezers). However, detection of ATP generated by a single F_1 is not easy: if we assume that three ATP molecules are synthesized in one turn of F_1 and if we rotate F_1 in the ATP synthesis direction at 10 Hz for 1 min, only 1800 ATP molecules will be synthesized. This amount of ATP

(3×10^{-21} mole) is too low to be detected by conventional detection method (such as luciferin–luciferase assay). However, if we can enclose a single F_1 and chemicals in a chamber with a volume of 6 fL, the 1800 ATP molecules correspond to a concentration of 0.5 μM. This concentration is sufficiently high for detection.

So, we enclosed single F_1 molecule into fL chamber and rotated it to the ATP synthesis direction using magnetic tweezers [Fig. 7(b)]. To estimate the number of ATP generated by the single F_1 molecule, we used a property of F_1. Similar to many other ATPases, ATP hydrolysis (and rotation) rate of F_1 obeys Michaelis–Menten kinetics,[33] and the rate is proportional to [ATP] at low concentration. Therefore, at low [ATP], the number of ATP molecules synthesized during forced rotations could be determined from the increase in the rotation rate.

Unexpectedly the mechano-chemical coupling ratio of $\alpha_3\beta_3\gamma$ subcomplex, that exhibits very high value when it hydrolyzes ATP (namely 3 ATP/turn), was found to be very low in the ATP-synthesis direction (around 10% or 0.3 ATP/turn) [Fig. 7(c), left]. However, when the ε subunit was reconstituted with $\alpha_3\beta_3\gamma$, the ratio increased significantly [Fig. 7(c), right]. Some molecules exhibited a very high efficiency (nearly 100%) and the average value reached 77% (2.3 ATP/turn). This result clearly indicates that the F_1 synthesizes ATP with a very high efficiency when bound to the ε, and a novel, unexpected role of this small subunit was revealed.

4. Perspectives

Examples described in this review are initial studies to investigate the feasibility of the fL chamber array. Although still at its infancy stage, the potential of the fL chamber arrays is evident. In addition to the examples shown here, the fL chamber array can be combined with many kinds of single-molecule methods based on optical microscopy, such as single-pair fluorescence resonance energy transfer,[34] fluorescence imaging with one-nanometer accuracy (so-called FIONA),[35] zero-mode waveguide,[36] and optical tweezers.[37]

The fL chamber array can be prepared by many kinds of materials other than PDMS and PAA, as well as gels like agarose. Furthermore, single living cells can also be easily enclosed. By culturing single cells in fL chambers, high throughput screening of drugs that are effective against the infectious bacteria and cancer cells can be achieved. By using the genome library of these cells, screening of the genes encoding for the proteins targeted by these drugs can be also achieved.

To implement and to integrate more advanced functions into the fL chamber arrays, further improvements, such as enclosure of different samples in individual chambers, rapid exchange of solution in individual chambers, and recovery of samples from individual chambers are required. For this purpose, we have recently developed water-in-oil type fL chamber array formed on hydrophobic/hydrophilic patterned surface.[38] By using oil (liquid) to isolate fL chambers containing aqueous solution, direct access to individual chambers became possible. Further applications of fL chamber array will be demonstrated in near future.

1) K. Svoboda, C. F. Schmidt, B. J. Schnapp, and S. M. Block: Nature **365** (1993) 721.
2) J. T. Finer, R. M. Simmons, and J. A. Spudich: Nature **368** (1994) 113.
3) T. Funatsu, Y. Harada, M. Tokunaga, K. Saito, and T. Yanagida: Nature **374** (1995) 555.
4) I. Sase, H. Miyata, J. E. Corrie, J. S. Craik, and K. Kinosita, Jr.: Biophys J. **69** (1995) 323.
5) *Single-Molecule Techniques; A Laboratory Manual*, ed. T. Ha and P. R. Selvin (Cold Spring Harbor Laboratory Press, New York, 2007).
6) *Single Molecule Dynamics in Life Science*, ed. T. Yanagida and Y. Ishii (Wiley-VCH, Weinheim, 2009).
7) H. Craighead: Nature **442** (2006) 387.
8) Y. Rondelez, G. Tresset, K. V. Tabata, H. Arata, H. Fujita, S. Takeuchi, and H. Noji: Nat. Biotechnol. **23** (2005) 361.
9) L. Lam, S. Sakakihara, K. Ishizuka, S. Takeuchi, and H. Noji: Lab Chip **7** (2007) 1738.
10) L. Lam, S. Sakakihara, K. Ishizuka, S. Takeuchi, H. F. Arata, H. Fujita, and H. Noji: Biomed. Microdevices **10** (2008) 539.
11) L. Lam, R. Iino, K. V. Tabata, and H. Noji: Anal. Bioanal. Chem. **391** (2008) 2423.
12) Y. Rondelez, G. Tresset, T. Nakashima, Y. Kato-Yamada, H. Fujita, S. Takeuchi, and H. Noji: Nature **433** (2005) 773.
13) R. Iino, Y. Rondelez, M. Yoshida, and H. Noji: J. Bioenerg. Biomembranes **37** (2005) 451.
14) G. M. Whitesides, E. Ostuni, S. Takayama, X. Jiang, and D. E. Ingber: Annu. Rev. Biomed. Eng. **3** (2001) 335.
15) B. Rotman, J. A. Zderic, and M. Edelstein: Proc. Natl. Acad. Sci. U.S.A. **50** (1963) 1.
16) M. Washizu and O. Kurosawa: IEEE Trans. Ind. Appl. **26** (1990) 1165.
17) M. Ueda: J. Biochem. Biophys. Methods **41** (1999) 153.
18) H. F. Arata, Y. Rondelez, H. Noji, and H. Fujita: Anal. Chem. **77** (2005) 4810.
19) H. Noji, R. Yasuda, M. Yoshida, and K. Kinosita, Jr.: Nature **386** (1997) 299.
20) M. Yoshida, E. Muneyuki, and T. Hisabori: Nat. Rev. Mol. Cell. Biol. **2** (2001) 669.
21) K. Kinosita, Jr., K. Adachi, and H. Itoh: Annu. Rev. Biophys. Biomol. Struct. **33** (2004) 245.
22) J. P. Abrahams, A. G. Leslie, R. Lutter, and J. E. Walker: Nature **370** (1994) 621.
23) T. Ariga, E. Muneyuki, and M. Yoshida: Nat. Struct. Mol. Biol. **14** (2007) 841.
24) T. Masaike, F. Koyama-Horibe, K. Oiwa, M. Yoshida, and T. Nishizaka: Nat. Struct. Mol. Biol. **15** (2008) 1326.
25) K. Adachi, H. Noji, and K. Kinosita, Jr.: Methods Enzymol. **361** (2003) 211.
26) R. Yasuda, H. Noji, K. Kinosita, Jr., and M. Yoshida: Cell **93** (1998) 1117.
27) R. Yasuda, H. Noji, M. Yoshida, K. Kinosita, Jr., and H. Itoh: Nature **410** (2001) 898.
28) K. Shimabukuro, R. Yasuda, E. Muneyuki, K. Y. Hara, K. Kinosita, Jr., and M. Yoshida: Proc. Natl. Acad. Sci. U.S.A. **100** (2003) 14731.
29) K. Adachi, K. Oiwa, T. Nishizaka, S. Furuike, H. Noji, H. Itoh, M. Yoshida, and K. Kinosita, Jr.: Cell **130** (2007) 309.
30) R. Watanabe, R. Iino, K. Shimabukuro, M. Yoshida, and H. Noji: EMBO Rep. **9** (2008) 84.
31) P. D. Boyer: Annu. Rev. Biochem. **66** (1997) 717.
32) H. Itoh, A. Takahashi, K. Adachi, H. Noji, R. Yasuda, M. Yoshida, and K. Kinosita: Nature **427** (2004) 465.
33) L. Michaelis and M. L. Menten: Biochem. Z. **49** (1913) 333 [in German].
34) R. Roy, S. Hohng, and T. Ha: Nat. Methods **5** (2008) 507.
35) A. Yildiz, J. N. Forkey, S. A. McKinney, T. Ha, Y. E. Goldman, and P. R. Selvin: Science **300** (2003) 2061.
36) M. J. Levene, J. Korlach, S. W. Turner, M. Foquet, H. G. Craighead, and W. W. Webb: Science **299** (2003) 682.
37) J. R. Moffitt, Y. R. Chemla, S. B. Smith, and C. Bustamante: Annu. Rev. Biochem. **77** (2008) 205.
38) S. Sakakihara, R. Iino, and H. Noji: unpublished results.